Nop10 Is a Conserved H/ACA snoRNP Molecular Adaptor[†]

Steve L. Reichow[‡] and Gabriele Varani*[,‡,§]

Department of Biochemistry, University of Washington, Box 357350, Seattle, Washington 98195-7350, and Department of Chemistry, University of Washington, Box 351700, Seattle, Washington 98195-1700

Received March 11, 2008; Revised Manuscript Received April 13, 2008

ABSTRACT: The H/ACA class of small nucleolar ribonucleoproteins (snoRNPs) is primarily responsible for catalyzing the isomerization of uridine to pseudouridine (Ψ) in ribosomal and other cellular RNAs. Each H/ACA snoRNP consist of four conserved proteins, Cbf5 (the Ψ-synthase), Gar1, Nhp2 (L7Ae in archaea) and Nop10, that assemble onto a unique RNA component (the snoRNA). The smallest of these proteins, Nop10 (∼7 kDa), has an essential role in the assembly and activity of these particles and binds directly to the Ψ-synthase to form the minimal active enzyme in archaea. To better understand the conserved function of this protein, we characterized the NMR structure and dynamics of Nop10 proteins from both archaea and yeast. We show that archaeal Nop10 contains a highly stable Zn^{2+} binding motif that is replaced in eukaryotes by a smaller meta-stable β-hairpin, while a highly conserved and conformationally dynamic linker connects these motifs to a nascent α-helical structure. Our structural analysis and NMR relaxation data show that these motifs do not interact with each other and tumble independently in solution. Several residues within the archaeal Nop10 Zn^{2+} binding motif have clear structural and functional roles and are conserved in eukaryotes, yet remain disordered in the free yeast Nop10. We propose that the dynamic structure of Nop10 facilitates an induced-fit recognition with the H/ACA Ψ-synthase and allows it to act as a molecular adaptor for guiding snoRNP assembly in similar fashion in all archaea and eukaryotic organisms.

The H/ACA small nucleolar ribonucleoproteins (snoRNPs[1]) are a highly conserved class of RNA−protein complexes found in eukaryotes and archaea that are responsible for catalyzing the isomerization of uridine to pseudouridine (Ψ). This ubiquitous post-transcriptional modification is thought to promote the folding and stability of the local RNA structure in the ribosome and other RNAs (*1*). Most H/ACA snoRNPs localize to the nucleolus in eukaryotic cells, the site of ribosome biogenesis, where they carry out catalysis at conserved sites of ribosomal RNA (rRNA) (*2*).

Each H/ACA snoRNP is defined by a single unique RNA component, the H/ACA snoRNA (*3–5*), that assembles with four highly conserved core protein subunits that are common to all H/ACA snoRNPs, known as Cbf5 (dyskerin or NAP57 in mammals), Gar1, Nhp2 (L7Ae in archaea), and Nop10 (*6–8*). Cbf5 is the Ψ-synthase responsible for catalyzing the isomerization reaction (*9–11*), while the three additional H/ACA-specific core proteins Gar1, Nhp2 and Nop10, are required for maturation, stability and nucleolar localization of the snoRNP (*12–17*). Individual H/ACA snoRNAs contain conserved sequence motifs (the H and ACA boxes) as well as unique internal sequence elements that contain base-pair complementarity to regions flanking their specific target, thus providing the particle with substrate specificity (*18–20*).

While most H/ACA snoRNA are programmed for guiding Ψ-synthesis, some eukaryotic H/ACA snoRNPs are non-catalytic, yet play critical biological roles. A subset of H/ACA snoRNPs is required for pre-rRNA cleavage steps during ribosome biogenesis (*21, 22*), apparently by acting as RNA folding chaperones. In higher eukaryotes, the H/ACA proteins associate with the RNA component of telomerase and are required for the stability and localization of this RNP (*23–25*). Mutations in the Ψ-synthase (*26*) as well as human Nop10 (*27*) have been linked to the rare genetic disorder dyskeratosis congenita (DC). Patients carrying this disease have aberrant telomerase activity and ribosome biogenesis (*28*).

Nop10 is a unique protein of ∼7 kDa that has been shown to play a central role in the assembly and activity of the H/ACA sno(s)RNPs. It binds directly to the Ψ-synthase in eukaryotes (*29, 30*) and archaea (*10, 31*), where this interaction is required for basal *in vitro* activity of the enzyme (*10*). Our structural studies of the archaeal Cbf5−Nop10 complex suggested that archaeal Nop10 might regulate the activity of Cbf5 by stabilizing residues at the catalytic site (*11*). In that same study, we showed by NMR perturbation analysis that Nop10 from archaea (aNop10) and yeast (yNop10) are both able to bind the archaeal Cbf5 protein. The recent X-ray crystallographic structure of an assembled archaeal H/ACA sRNP contains the four core proteins assembled onto a guide sRNA (*32*), and revealed additional inter-RNP interactions involving Nop10 that support a central functional role of Nop10 in particle assembly.

[†] This work was funded by NIH-NCI.

* Corresponding author. E-mail: varani@chem.washington.edu. Phone: 206-543-7113. Fax: 206-685-8665.

[‡] Department of Biochemistry.

[§] Department of Chemistry.

[1] Abbreviations: snoRNP, small nucleolar ribonuclear protein; sRNP, small ribonuclear protein; NMR, nuclear magnetic resonance; HSQC, heteronuclear single quantum coherence; NOE, nuclear overhauser effect.

10.1021/bi800418p CCC: $40.75
Published on Web 05/13/2008

To better understand the conserved structural and dynamic properties of Nop10 and to gain insight into the mechanism by which Nop10 facilitates sno(s)RNP assembly, we have conducted a side-by-side structural analysis of the archaeal and eukaryotic Nop10 proteins. We have also characterized by NMR the backbone dynamics of both proteins using relaxation studies. Although Nop10 from archaea and eukaryotes perform a conserved functional role in the recognition of Cbf5, the proteins from these two species contain divergent structural and dynamic features. While archaea Nop10 proteins contain a compact Zn^{2+}-binding domain that is involved in the recognition of archaeal Cbf5, eukaryotic Nop10 proteins have instead a smaller metastable β-hairpin motif. Sequence analysis identified several residues with clear structural and functional roles within the archaea Nop10 Zn^{2+} motif that are conserved in eukaryotic proteins, yet remain completely disordered in the free yNop10 protein. From the insights gained from our structural and dynamics studies and from the recently reported X-ray crystallographic structure of the fully assembled archaea H/ACA sRNP, we propose that the conserved features of Nop10 allow this protein to serve as a molecular adaptor for the Cbf5 Ψ-synthase that facilitates sno(s)RNP assembly in a highly similar fashion in both archaeal and eukaryotic organisms.

EXPERIMENTAL PROCEDURES

Procedures for the expression, purification and NMR structure determination of Nop10 from the archaea *Methanococcus jannaschii* (aNop10) and yeast *Saccharomyces cerevisiae* (yNop10) have been described in detail previously (*11*). Freshly purified samples of unlabeled or uniformly ^{15}N-labeled aNop10 and yNop10 (~1 mM) were prepared as described for NMR dynamics measurements in (8% v/v) D_2O containing 50 mM (^2D) NaOAc (pH-5.0) and 100 mM KCl. Archaea Nop10 samples were supplemented with either 100 μM excess $ZnCl_2$ or 25 mM EDTA and 2 mM (^2D) DTT.

Standard triple resonance experiments (HNCO, HNCA, HN(CO)CACB, HN(CO)CA, HBHA(CO)HN and HCCH-TOCSY) (*33*) were used to obtain nearly complete assignments for both aNop10 and yNop10. Structural restraints were obtained through heteronuclear ^{13}C- and ^{15}N-edited 3D experiments and homonuclear NOESY experiments collected with mixing times of 120 ms (aNop10) and 100 ms (yNop10). NOE assignments and structure calculations were performed using combined automated and manual methods in CYANA (*34*). Torsion angle restraints were included for ϕ/φ angles according to TALOS (*35*). Hydrogen bonding constraints were derived from amide D_2O protection data. Initial structure refinement of aNop10 used only these experimental restraints and clearly defined the four conserved cysteine side chain conformations, which were clustered together in a tetrahedral arrangement that unmistakably identified a single Zn^{2+} binding site. Therefore, during the final stage of refinement of aNop10, a Zn^{2+} ion was added and constrained to each zinc-chelating Sγ atoms (Sγ-Zn^{2+}, 2.6Å), and tetrahedral geometry between the four Sγ atoms was enforced (Sγ−Sγ, 4 Å). Final refinement for both aNop10 and yNop10 yielded no distant restraint violation >0.2 Å and >99% of residues in allowed regions of the Ramachandran plot for both polypeptides.

NMR dynamics studies for both Nop10 proteins were carried out using standard pulse sequences to record ^{15}N heteronuclear NOEs (Het-NOE), T_1 and T_2 measurements (*36*) at 298 K on a Bruker Avance 500 MHz spectrometer equipped with a *z*-axis pulsed-field gradient triple resonance probe. Experiments were collected with spectral widths of 1822.490 and 6009.615 Hz in the ^{15}N and ^1H dimensions, respectively. For the heteronuclear NOE measurements, two spectra were recorded with and without proton saturation, which was achieved by application of ^1H 120° pulses every 5 ms. Spectra recorded with proton saturation utilized a two second recycle delay followed by a three second period of saturation, while spectra recorded in the absence of saturation employed a recycle delay of five seconds. Heteronuclear NOE values were calculated from the ratio of peak heights with and without proton saturation. Uncertainties in these measurements were estimated from the base plane noise in ^{15}N-HSQC spectra recorded with and without proton saturation. For both aNop10 and yNop10, delays of 0.010, 0.020 (×2), 0.40, 0.70, 0.140, 0.240, 0.350, 0.480 (×2) 0.600 s were used for the T_1 experiments. T_2 values were measured from spectra recorded with delays of 0.008, 0.016, 0.024 (×2), 0.040, 0.056, 0.080, 0.112, 0.144 (×2) and 0.192 s, respectively. The relaxation delay was 1.9 s for each experimental set. Peak heights were calculated for every assigned peak in the T_1 and T_2 spectra and fit to an exponential curve, $I(t) = I(0)\exp(-t/T_{1,2})$ where $I(0)$ is the initial peak intensity and t is the delay time, using the Sparky relaxation fit software. Rotational correlation times (τ_c) were calculated from T_1/T_2 ratios (*37*).

In order to study the structural effects of Zn^{2+} on aNop10, unlabeled or uniformly ^{15}N labeled aNop10 samples were exchanged into buffers containing either $ZnCl_2$ or a molar excess of EDTA by dialysis, and ^{15}N-heteronuclear single quantum coherence (HSQC) spectra and 2D $^1H-^1H$ NOESY experiments were collected at 298 K on the Bruker 500 MHz spectrometer. NOESY experiments were collected with mixing times (τ_{mix}) of 120 ms. HSQC and NOESY spectra were analyzed for chemical shift perturbations and global structural changes to aNop10 that occurred in response to the presence or absence of Zn^{2+}. All NMR data were processed with NMRPipe/NMRDraw (*38*) and analyzed using Sparky (T. D. Goddard and D. G. Kneller, University of California, San Francisco). Atomic coordinates for aNop10 (PDB accession number 2AQC), yNop10 (PDB accession number 2AQA), the aCbf5-aNop10 complex (PDB accession number 2APO) (*11*), and the H/ACA sRNP (PDB accession number 2HVY (*32*)) were visualized and prepared for illustration using UCSF Chimera (*39*). A surface electrostatic potential map of the aNop10 Zn^{2+} binding domain was calculated and displayed using MolMol (*40*).

RESULTS

Comparative Analysis of Archaeal and Eukaryotic Nop10 NMR Structures. The structures of Nop10 from the archaea *Methanococcus jannaschii* (aNop10) and yeast *Saccharomyces cerevisiae* (yNop10) were determined by NMR. Structure calculation and refinement was done in CYANA v2.0 (*34*) using atomic distance restraints derived from NOE intensities, ϕ/φ restraints derived from chemical shift values and TALOS (*35*) and hydrogen bond restraints for amides protected from D_2O exchange. The atomic coordinates of

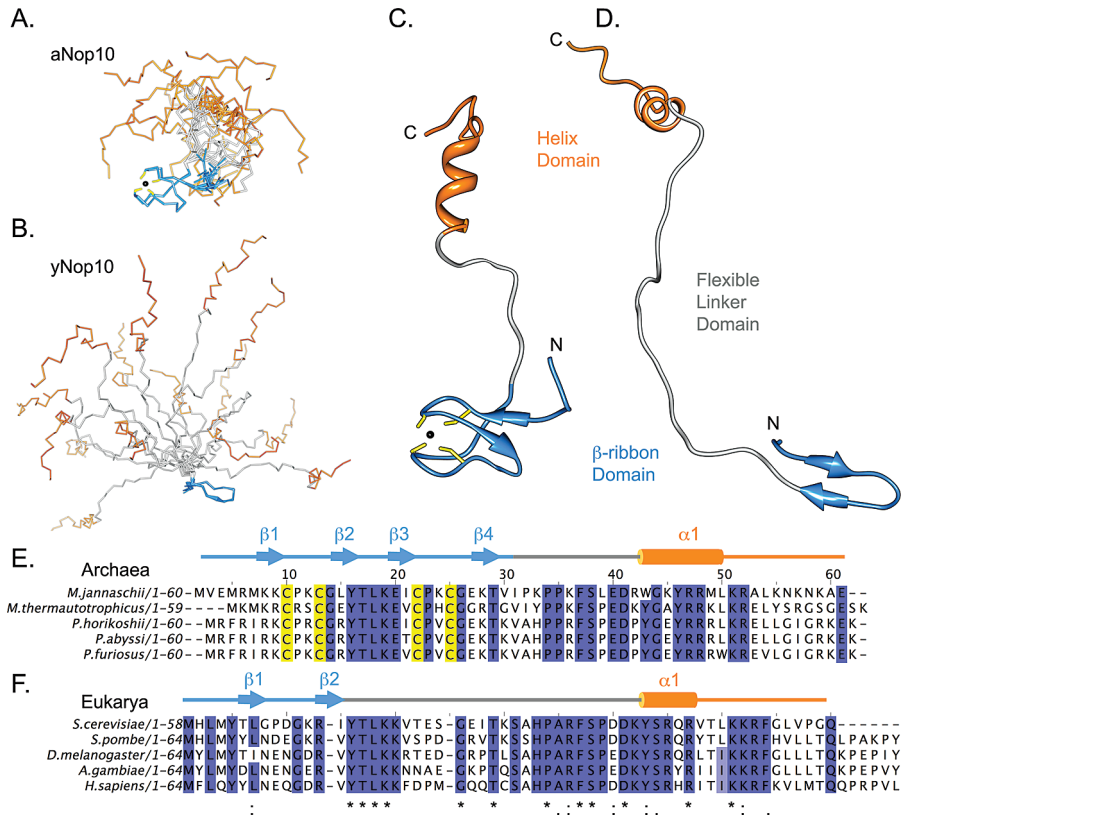

FIGURE 1: Structure of Nop10 from archaea and eukaryotes. Nop10 from archaea (aNop10) and yeast (yNop10) contain both conserved and divergent structural features that correspond to sequence differences between archaea and eukaryotes. (A and B) Cα trace of 15 low-energy NMR structures of aNop10 and yNop10, respectively. Structures are colored according to the three structural domains: N-terminal β-ribbon (cyan), internal flexible linker (gray), and C-terminal helix (orange). The structural ensembles have been superimposed over the respective β-ribbon domains; the N- and C-terminal domains do not interact. The aNop10 protein binds a single Zn^{2+} ion (black) through four conserved cysteine side chains (yellow). Eukaryotic Nop10 proteins have replaced this N-terminal domain with a smaller β-ribbon. (C and D) Representative ribbon structures of aNop10 and yNop10, respectively. (E and F) Primary sequence alignment vs secondary structure for Nop10 proteins from archaea (E) and eukaryotes (F). Conserved residues are indicated in blue, and archaeal Zn^{2+} binding cysteines in yellow. Symbols (bottom) represent conservation between both archaea and eukaryotes.

the Nop10 NMR structures have been previously reported with the structure of the archaeal Cbf5-Nop10 complex (*11*). Here we conduct a side-by-side characterization of the NMR structures of these two paralogous Nop10 proteins in their free form to gain functional insight into the evolution of this protein between archaea and eukaryotes.

Both aNop10 and yNop10 contained a low number of long distance, structurally meaningful NOE distance information compared to globular folded proteins of similar size, and those NOEs were unevenly distributed along the polypeptide chains. For both proteins, the highest NOE density localized to residues in the N-terminal region and within a short stretch of residues near the C-terminus. During structure refinement of aNop10 four cysteine side chains were found to be clearly arranged in a tetrahedral geometry defining a single Zn^{2+} binding site. Therefore, during the final refinement stages, a Zn^{2+} ion was added to the model and constraints between the four conserved zinc-ligating Sγ atoms and the Zn^{2+} ion were applied to the aNop10 structure.

The Cα traces for 15 lowest energy NMR models for aNop10 and yNop10 are shown in Figure 1A and B respectively. These structures show that both aNop10 and yNop10 adopt two independent structural domains, a highly ordered N-terminal β-ribbon domain and a nascent C-terminal helix. A conformationally flexible linker connects these two motifs. Each of these three domains is colored in the same way in each model; they are shown superimposed over the N-terminal β-ribbon domains. For both aNop10 and yNop10, the β-ribbon domains are the best-defined region of the NMR structure ensembles, owing to the rich amount of NOE data found within these structured regions of the protein (backbone root mean squared deviation, rmsd; aNop10 ~0.11 Å, residues 6−31; yNop10 0.22 Å, residues 5−15).

Representative low energy models of aNop10 and yNop10 are displayed as ribbon structures in Figure 1C and D. These structures juxtapose regions of conserved and species-specific structural motifs that correspond to regions of primary sequence conservation and variation, respectively. The major structural difference between aNop10 and yNop10 is located within their respective β-ribbon domains. The aNop10 structure contains two orthogonally stacked β-hairpin motifs (β1/2 and β3/4) with a single Zn^{2+} ion (black) bound at the center by four cysteine side chains (yellow). This motif is very well-defined by a dense network of NOE restraints and hydrogen bonding interactions. The β3/4 hairpin of the aNop10 N-terminal motif is slightly distorted between residues Lys27 and Thr28 (Lys27 φ values = −50°) on the β4 strand and is therefore not recognized as a β-strand by secondary structure recognition algorithms (*41*). The distortion in β4 facilitates cross-strand hydrogen bonding with β1, while maintaining the β-hairpin hydrogen bond network with β3. The four cysteine residues are displayed by each of the β-ribbons and arranged with a tetrahedral geometry around

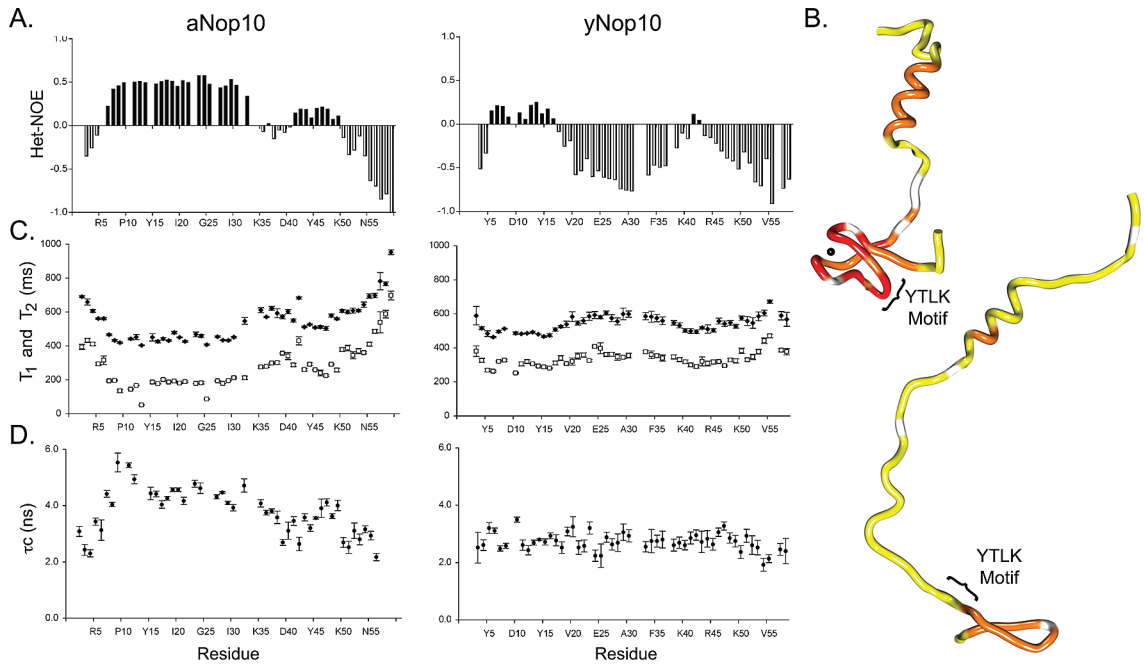

FIGURE 2: Dynamics of Nop10 as studied by NMR. Nop10 from archaea and yeast share conserved dynamic profiles. (A) ^{15}N heteronuclear NOE (Het-NOE) values for aNop10 (left) and yNop10 (right) are plotted against amino acid sequence. Het-NOE values are arbitrarily classified as 1.0−0.5 ordered, 0.5−0.0 partially ordered, <0.0 disordered. The Het-NOE values for aNop10 and yNop10 have been mapped to the tube representation of aNop10 and yNop10, and are colored according to these classes (B). In both proteins, the β-ribbon domain is the most stable. The low Het-NOE values over the C-terminal helical domains indicate significant pico- to nanosecond dynamics. A highly dynamic linker connects the two terminal domains of Nop10. The position of the conserved YTLK tetrapeptide motif described in the text is labeled. (C) T_1 and T_2 values plotted against aNop10 and yNop10 amino acid sequence correlate with the overall trends in Het-NOEs. Error bars indicate uncertainty of the primary data (see Experimental Procedures). (D) Rotational correlation coefficients (τ_c) values determined by the T_1/T_2 method for aNop10 and yNop10 plotted against amino acid sequence indicate the N- and C- terminal Nop10 domains tumble independently.

the Zn^{2+} ion. These Zn^{2+} chelating residues are conserved among archaea Nop10 proteins (see alignment Figure 1E). Eukaryotic Nop10 proteins have replaced these Zn^{2+} chelating residues (see alignment Figure 1F) and therefore do no have the ability to bind Zn^{2+}. In spite of this divergence, yNop10 has maintained structural homology with the N-terminal β-hairpin (β1/2). However, the yNop10 β1/2 hairpin is more loosely defined by NOE constraints than the β-ribbon domain of aNop10. The NMR data suggest that this is due to the lack of conformational stability of this small motif. For example, although the expected cross-strand Hα-Hα NOE signatures of antiparallel β-sheet were clearly identified, the intensities were weaker then expected. In addition, the expected cross-strand amide protection from D_2O exchange could not be observed. The residues directly following the β-hairpin motif are unstructured and contribute to the central linker domain in the free yNop10 protein.

The central and C-terminal regions of Nop10 proteins are the most highly conserved in sequence across all species, yet these regions of aNop10 and yNop10 are largely unstructured in the free proteins. The internal linkers of aNop10 and yNop10 did not contain any structurally meaningful NOE or structurally useful chemical shift information. In addition, the amide resonances in this region of the protein were marked by strong sequential αN NOEs, indicative of an extended conformation. The Nop10 C-terminal α-helices are only loosely defined in the NMR structures. This was due to a low level of NOE and chemical shift information and the complete absence of hydrogen bond restraints that could be derived from the D_2O protection studies. Therefore, in the final structural ensembles only 18/20 and 16/20 structures yielded consistent helical conformations for aNop10 and yNop10, respectively. Satisfactorily, residues containing consistent helical character in the structural ensemble map to homologous positions of the aNop10 and yNop10 sequences (Figure 1E and F). The Nop10 helical residues displayed a combination of weak medium-range (i, i_{+2-4}) Hα−HN NOE signatures of α-helical conformation, as well as strong sequential (i, i_{+1}) Hα−HN NOE signatures of extended conformations. Taken together, these observations suggest the presence of conformational exchange between helical and extended states within the C-terminal domain of Nop10 that occurs on the NMR time-scale when these proteins are free in solution.

Backbone Dynamics of Archaeal and Eukaryotic Nop10. The NMR structures of the archaeal aNop10 and eukaryotic yNop10 proteins contain conserved regions that are intrinsically unstructured or loosely defined, and indicate that the two terminal domains of Nop10 are structurally independent. To better understand how these features may play a functional role in binding to the Ψ-synthase and in sno-(s)RNP assembly, we characterized the NMR backbone dynamics by collecting ^{15}N heteronuclear NOE, T_1 and T_2 measurements for both Nop10 proteins. ^{15}N heteronuclear NOE (Het-NOE) values for aNop10 and yNop10 are plotted against their primary sequence in Figure 2A. Since the Het-NOE is sensitive to internal motions on the pico- to nanosecond time scale, these values can be used to judge relative conformational stability.

We arbitrarily define Het-NOE values as >0.5 ordered, 0.5−0.0 partially ordered, <0.0 disordered. The Het-NOE values for aNop10 and yNop10 categorized that way and

colored according to this definition are shown in Figure 2B. The most striking feature is the similarity in the overall profile of Het-NOE values between the two proteins. As also indicated by the NMR structural data, the most stable regions of both proteins correspond to their respective N-terminal β-ribbon domains. Het-NOE values for the yNop10 β-hairpin motif ($\sim$0.2) are notably low and smaller than the values for the aNop10 β-ribbon domain ($\sim$0.5), which is consistent with the disparity in structurally meaningful NOEs and amide protection from D_2O exchange. Within the C-terminal domains, the highest Het-NOE values ($\sim$0.1−0.2) belong to the nascent α-helical regions: Arg41−Leu49 of aNop10 and Tyr41−Ser42 of yNop10, respectively. These low values indicate significant fast motion and explain the weak α-helical NOE intensities for these residues. Het-NOE values of residues in the internal linkers of both proteins are all negative, consistent with the lack of any structurally meaningful NOEs for these residues. In general, the trends in Het-NOE values for both aNop10 and yNop10 match the conformational dynamics indicated by the NOE data used for structure calculation.

Plots of T_1 and T_2 values versus the primary sequences of aNop10 and yNop10 reveal profiles that correspond with the overall profile of Het-NOE values as well; regions of low Het-NOE were matched by large T_1 and T_2 values (Figure 2C). For aNop10, T_1 and T_2 values were about 445 and 170 ms over the β-ribbon domain, and 545 and 280 ms over the C-terminal α-helical residues, respectively. For yNop10, T_1 and T_2 values were 490 and 290 ms over the β-hairpin motif and 535 and 305 ms over the nascent helix, respectively. Despite the large amount of motions, the data for both proteins were surprisingly good, with average errors for T_1 and T_2 values over the regions of secondary structure of only $\sim$1.5−2% and $\sim$3−5%, respectively. Large T_1 and T_2 values were obtained from residues within the internal linker domain and termini of both Nop10 proteins, as expected for unstructured regions with fast-motions. Relaxation rates for the C-terminal helical residues are distinctively shorter than the residues flanking them, indicating that fast-motions are quenched by the nascent secondary structural interactions that were indicated by the described NOE patterns and intensities.

The NMR structural studies suggest the N- and C-terminal domains of Nop10 are structurally independent in solution. To support this model, T_1/T_2 ratios were used to estimate rotational correlation times for aNop10 and yNop10 (Figure 2D). The rotational correlation time (τ_c) is a measure of the overall tumbling rate of a molecule, and is therefore sensitive to molecular size and shape. For a globular protein the size of Nop10 ($\sim$7 kDa), τ_c is expected to be $\sim$5.5 ns (*42*). For aNop10, average τ_c values of the N- and C-terminal motifs were 4.9 and 3.5 ns, respectively. That these values differ significantly and are lower than expected is in agreement with the two domains tumbling independently. For yNop10, τ_c values are even smaller, 2.9 and 3.0 ns over the N- and C-terminal domains, respectively. The similar τ_c values over these two domains of yNop10 are consistent with their similar sizes. Together, these data support our structural models, and are consistent with the lack of any long-range NOEs that could be identified between the Nop10 β-ribbon and α-helical domains.

Characterization of the Nop10 β-Ribbon Domains. The major differences in both structure and dynamics between aNop10 and yNop10 are found in their respective N-terminal β-ribbon domains. However, several residues within these domains are highly conserved between archaea and eukaryotes. The β-ribbon domain of aNop10 proteins adopts a minimalist version of the consensus zinc ribbon motif ($CX_2CX_{(n)}CX_2C$ topology, where X is any amino acid), one the most common class of zinc-binding motifs (*43*). With the exception of the paired cysteines, there is very little sequence homology between different families of proteins harboring this motif. The number of residues between the two pairs of cysteines can vary significantly, both in length and sequence and may include a complete domain insertion. In the compact aNop10 zinc ribbon motif, the fold is stabilized by the two β-turns in the aNop10, which adopt classical zinc "knuckle" structures. This type of turn is typified by a positive ϕ angle at the glycine residue directly following the second cytsteine and by characteristic backbone hydrogen bond interactions with the cysteine thiols (Figure 3A). In aNop10 proteins, the two cysteine pairs are separated by only 8 residues; this is the minimal number required to form a β-strand and a highly ordered turn (Turn II) while facilitating the orthogonal placement of the two β-hairpins. The core of the compact aNop10 zinc ribbon domain consists primarily of the four cysteine side chains and the Zn^{2+} ion. In addition, the side chain γ-methyls from two highly conserved threonine residues, Thr16 on β2 and Thr28 on β4, insert directly behind the zinc binding site and contributing to core packing interactions (Figure 3B). Packing of the side chain of Thr28 is facilitated by the backbone distortion in β4 that was described previously. Thr16 contributes to the stability of the highly ordered Turn II as well through a side chain hydrogen bond with Lys18 (Figure 3B).

When bound to Zn^{2+}, the aNop10 β-ribbon motif adopts a stable conformation with the majority of residues exposed to solvent and involved in the recognition of the archaeal H/ACA Ψ-synthase, aCbf5. The surface electrostatic potential map of the aNop10 zinc ribbon domain reveals two distinctively different faces, a polar face (β4/1) and a hydrophobic face (β2/3) (Figure 3C and D, respectively). Among archaeal species, residues contributing to the polar face are not well conserved in identity, but share conserved charges. The hydrophobic surface is composed of residues from a highly conserved YTLK tetrapeptide motif, which is involved in the recognition of the archaeal Ψ-synthase, aCbf5. A thiomethyl side chain from Met6 on β1 contributes to this hydrophobic surface patch as well. This residue is conserved as methionine among Nop10 proteins or replaced by a similar hydrophobic side chain. In the crystallographic structure of the aCbf5−aNop10 complex, the hydrophobic face of the aNop10 zinc ribbon motif forms van der Waals interactions with the Ψ-synthase, while the polar face of this domain remains solvent exposed (*11, 44*). A superposition of the free and aCbf5-bound aNop10 zinc ribbon domain (*11, 44*) shows that, with the exception of some minor side chain reorientations, this motif undergoes minimal structural changes upon binding the Ψ-synthase (Cα root-mean-square deviation = 0.813 Å, Figure 3E), consistent with the stability of this domain that was indicated by the higher Het-NOE values.

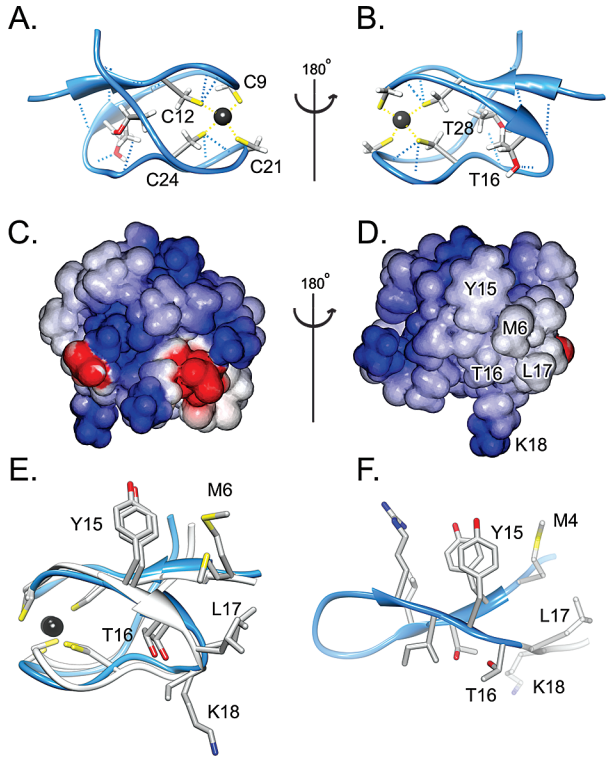

FIGURE 3: Characterization of the Nop10 β-ribbon domains. (A and B) The aNop10 zinc binding β-ribbon domain; core side chains are shown and labeled (colored by heteroatom). Numerous hydrogen bonds (dashed blue lines) stabilize this compact motif. (C and D) Electrostatic surface representation of the protein's structure (positive, blue; negative, red; neutral, white); residues on β1 and β4 contribute to the variable hydrophilic surface (C). On the opposite face of the motif (D), the strictly conserved Nop10 YTLK sequence (labeled, see Figure 1) connecting β2 and β3 contribute to a hydrophobic patch; Met6 is located on β1 and is largely conserved. These residues are involved in recognition of the archaeal Ψ-synthase, Cbf5. (E) Superposition of free (blue) and Cbf5-bound aNop10 zinc ribbon domains (white, PDB accession number 2APO) shows that only minor structural changes occur upon binding of Cbf5 (Cα rmsd, 0.813 Å). Side chains are represented by heavy atoms and colored as in A and B. In contrast to the rigid archaeal motif, the yNop10 β-ribbon motif is stabilized only by weak cross-strand side chain interactions (F). The same residues involved in the archaeal Cbf5 interaction are unstructured in yNop10 (unstructured residues colored transparently).

Unlike the rigid archaeal β-ribbon motif, the eukaryotic Nop10 N-terminal β-ribbon motif is only metastable, as shown by the low Het-NOE values. The small yNop10 hairpin motif appears to be maintained by cross-strand side chain-side chain van der Waals interactions (Figure 3F). Notably, however, yNop10 shares many residues with aNop10 that have important structural and functional roles, including the two β-turn glycines, the two core threonines, as well as the conserved YTLK tetrapeptide motif described above (see alignments in Figure 1). In stark contrast, however, these residues are primarily unstructured in the eukaryotic protein. The N-terminal YTLK sequence motif is conserved among all Nop10 proteins and is critical for both the structure and function of aNop10. However, with the exception of Tyr15, the corresponding residues in yNop10 remain conformationally undefined in the eukaryotic protein (labeled in Figure 3F). Presumably, these conserved residues have retained a functional role in eukaryotic Cbf5 recognition without the requirement for conformational stability.

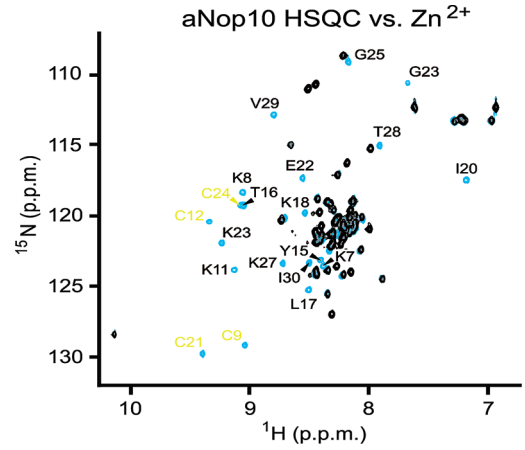

FIGURE 4: Zn^{2+} dependence of the folding of archaea Nop10. ^{15}N-HSQC spectra of aNop10 in the presence of Zn^{2+} (blue) and upon treatment with molar excess of EDTA (black). All resonances showing significant changes are from the zinc ribbon domain (labeled).

Folding of the Archaea Nop10 β-Ribbon Domain Requires Zn^{2+}. The observation that eukaryotic Nop10 proteins share many of the residues that play an important structural role in aNop10, yet these same residues are largely unstructured in yNop10, suggested that Zn^{2+} binding plays a primary role in the conformational stability of the aNop10 motif. In fact, under reducing conditions, the ^{15}N HSQC of aNop10 displays a mixture of well-dispersed and random-coil amide resonance values, as expected from the mixed folded/unfolded state of the aNop10 structure (Figure 4, blue). The most dispersed resonances in the ^{15}N-HSQC correspond to residues within the zinc ribbon domain of aNop10. When aNop10 is exchanged to buffer containing an excess of EDTA, the ^{15}N-HSQC spectrum shows a drastic collapse in ^{1}H dispersion to near random coil values (Figure 4, black). The aNop10 amide resonances showing significant changes in chemical shift in response to Zn^{2+} binding could all be assigned to residues within the zinc ribbon motif of Nop10, including the four cysteines responsible for chelating Zn^{2+} (labeled in Figure 4). The zinc-bound aNop10 ^{15}N-HSQC spectra could be recovered by returning the protein to buffer containing Zn^{2+} but no EDTA, demonstrating reversibility of the aNop10 zinc dependent fold. The zinc dependence of the ^{1}H−^{15}N HSQC chemical shift dispersion for aNop10 is most likely a consequence of the β-ribbon domain unfolding upon removal of Zn^{2+} ions. Analysis of aNop10 ^{1}H−^{1}H NOESY spectra collected under these conditions (data not shown) supports this assessment and is consistent with the minimal core packing interactions of this small domain. It is clear from these results that the free aNop10 protein requires Zn^{2+} binding to maintain the conformational rigidity of its β-ribbon motif.

DISCUSSION

Nop10 Dynamics and Cbf5 Recognition. The side-by-side analysis of the structure and dynamics of the H/ACA core protein Nop10 from archaea and yeast has shown that these proteins share a similar overall structural and dynamic profile. The N-terminal domain of archaeal Nop10 proteins contains a minimal zinc ribbon motif that requires Zn^{2+} for its structural integrity. Although eukaryotic Nop10 proteins have

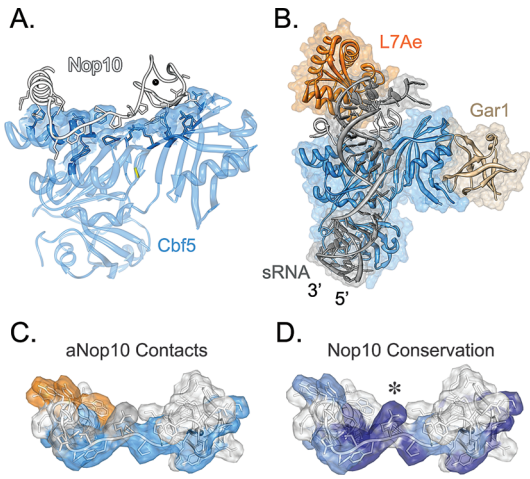

FIGURE 5: Nop10 has a conserved functional role in sno(s)RNP assembly. (A) The crystallographic structure of the archaeal Cbf5-Nop10 complex (PDB accession number 2APO (*11*)). The interaction between aNop10 (white) and aCbf5 (blue) is expansive and involves highly conserved residues from both proteins (interacting side chains and aCbf5 contacts are surface displayed). The aNop10 interactions are thought to buttress the aCbf5 active site (yellow). (B) The crystallographic structure of an assembled archaeal H/ACA sRNP (PDB accession number 2HVY (*32*)). The core proteins are colored as follows: Cbf5, blue; Gar1, brown; L7Ae, orange; Nop10, white; the H/ACA sRNA is in gray. (C) Contact surface representation of aNop10 colored as in (B). Nop10 makes extensive contacts with Cbf5 that span all three domains. The C-terminal domain additionally packs against L7Ae and the central linker domain makes contacts with the upper-stem of the sRNA. (D) Surface representation of Nop10 highlighting conserved amino acids. Residues of Nop10 conserved from archaea to eukaryotes are colored (dark blue = most conserved). These residues almost perfectly overlap with those involved in sRNP interaction in the archaeal complex. The human Nop10 mutation (R34W) linked to the genetic disorder dyskeratosis congentia maps to the RNA binding site of aNop10 (∗).

replaced this Zn^{2+} binding domain with a less well-structured domain, several amino acids that play important structural and functional roles in the archaea Nop10 fold have been conserved to allow induced-fit recognition with the very well-conserved H/ACA Ψ-synthase Cbf5. We have previously shown by NMR perturbation studies that both aNop10 and yNop10 can bind directly to aCbf5 through an interaction involving the entire molecule, suggesting a highly conserved recognition mechanism.

Our NMR studies reported here show that, in the absence of Cbf5, Nop10 proteins from both archaeal and yeast adopt a highly dynamic conformation with multiple populated states. In the crystal structures of the archaeal aCbf5-aNop10 complex (*11, 44*), the conformation of aNop10 is stabilized beyond the conserved features seen in the free protein and molded by numerous interactions with the catalytic domain of the Ψ-synthase that span nearly the entire length of Nop10 and involve highly conserved residues from both proteins (Figure 5A). The N- and C-terminal domains of aNop10 are separated by the ~20 Å linker, which buttresses the back of the Cbf5 active site (yellow in Figure 5A) (*11*). The highly conserved tetrapeptide sequence (YTLK motif) plays a critical role in the structure of aNop10 and provides a hydrophobic surface for interaction with aCbf5. Surprisingly, these same residues are unstructured in the yeast Nop10 protein. Our previous NMR perturbation analysis showed that these same residues in yNop10 undergo drastic chemical shift changes upon binding the archaeal Cbf5 protein. Therefore, we propose that the YTLK motif plays a similar functional role in eukaryotic Nop10 proteins by making comparable hydrophobic interactions with the eukaryotic Ψ-synthase. We also suggest that binding to Cbf5 induces a structure in the eukaryotic Nop10 N-terminal domain that is structurally similar to the zinc-bound topology observed in the aNop10 structure. This suggestion would rationalize the conservation of residues that have a clear structural role in aNop10, yet are unstructured in the free yNop10. These hypotheses are supported by biochemical studies that show that an archaeal Nop10 mutant incapable of binding Zn^{2+} retains the ability to assemble into a H/ACA sRNP particle with wild-type Ψ-activity (*44*). It is therefore likely that archaeal Nop10 proteins require the conformational stability provided by Zn^{2+} binding to function under the extreme physiological conditions in which these species thrive. Without such stringent requirements for stability, the metastable β-ribbon motif found in eukaryotic Nop10 could provide some functional advantage, perhaps by providing the plasticity required to accommodate the catalytic mechanism of eukaryotic Ψ-synthases. The structural and dynamic differences between Nop10 from archaea and eukaryotes may also reflect a difference in sno(s)RNP particle assembly. In eukaryotes, the assembly of H/ACA snoRNPs occurs cotranscriptionally (*45, 46*); therefore, eukaryotic Nop10 proteins may be stabilized early on during particle biosynthesis by protein−protein interactions. However, we note it is currently not known if the archaea follow a similar assembly pathway *in vivo*.

We found no evidence at all that the N- and C-terminal domains of Nop10 interact with each other. In fact, backbone NMR dynamics measurements show conclusively that these domains tumble independently of each other. This result is in contrast to another NMR study of yNop10, which reportedly observed long-range NOE connectivity between the N-terminal β-hairpin and C-terminal α-helix. This was surprising, because the T_1/T_2 values reported over these two domains were also consistent with independent tumbling (*47*). We did not observe any interdomain NOEs in our studies; most importantly, the NMR relaxation data are unambiguous in negating the possible formation of stable interdomain interactions. Perhaps the 10 °C temperature differences between these two studies can be attributed to these differences. However, it is highly unlikely that any interdomain contact is relevant to the function of Nop10. In the aCbf5-aNop10 complex, the two domains are separated by ~20 Å. Therefore, any transient interactions that may occur between the yNop10 domains cannot be preserved in the complex with Cbf5.

Structural Conservation of Nop10 and sno(s)RNP Assembly. The H/ACA enzyme Cbf5 is unique among other Ψ-synthases in that it requires the assembly of accessory proteins and a guide RNA for catalysis (*48*). A recent crystallographic structure for a fully assembled H/ACA sRNP from the archaea *Pyrococcus furiosis* (*32*) (Figure 5B) contains each of the core proteins: aCbf5 (cyan), aGar1 (brown), L7Ae (orange) and aNop10 (white), assembled onto a guide H/ACA sRNA (gray). The structure illustrates the structural role of Nop10 in facilitating intermolecular interactions between the Ψ-synthase and the other core sRNP components, and provides insight into the structural and

functional roles of Nop10 in eukaryotic snoRNP assembly. Nearly the entire surface of aNop10 is utilized for intermolecular interactions in the archaea H/ACA sRNP (Figure 5C). In addition to the expansive interaction with Cbf5, the central linker domain forms salt bridges with the upper stem of the H/ACA sRNA, and the C-terminal helix mediates packing interactions with L7Ae.

Strikingly, nearly every residue of aNop10 that is involved in intra-sRNP contacts corresponds to the residues that have been conserved in eukaryotic Nop10 proteins (Figure 5D). This remarkable conservation strongly supports a conserved functional and structural role of Nop10 in the assembled snoRNP as a molecular adaptor required for snoRNP assembly and function. This central role in snoRNP assembly and function is further supported by several biochemical studies. The mammalian H/ACA Ψ-synthase (NAP57) binds Nhp2 (the eukaryotic L7Ae orthologue) in a Nop10 dependent fashion to form a protein-only core complex (*30*). In addition, early studies using assembled H/ACA snoRNP particles showed that Nop10 can be efficiently cross-linked to the snoRNA (*49*). Furthermore, a mutation in Nop10 was recently identified in a family of patients with the autosomal recessive form of dyskeratosis congenita (DC) (*27*), an inherited genetic disorder linked to mutations in the H/ACA Ψ-synthase (dyskerin) and the H/ACA domain of telelomerase RNA (TR) characterized by impaired telomerase activity and/or ribosome biogenesis (*28*). Several of the DC mutations in dyskerin map to the RNA binding surface of the aCbf5 structure, suggesting that the disease phenotype is a result of impaired RNA binding (*11*). Similarly, the Nop10 DC mutant corresponds to a well-conserved residue Arg34 in the *P. furiosus* aNop10 structure (asterisk in Figure 4C) that interacts with the minor groove of the sRNA upper stem, suggesting a similar biochemical defect in RNA binding resulting from this mutation.

ACKNOWLEDGMENT

We thank Adrian Ferre D'Amare and Tomoko Hamma for providing us the expression plasmid for aNop10 and for helpful discussions during the preparation of this manuscript.

REFERENCES

1. Helm, M. (2006) Post-transcriptional nucleotide modification and alternative folding of RNA. *Nucleic Acids Res. 34*, 721–733.
2. Decatur, W. A., and Fournier, M. J. (2002) rRNA modifications and ribosome function. *Trends Biochem. Sci. 27*, 344–351.
3. Maxwell, E. S., and Fournier, M. J. (1995) The small nucleolar RNAs. *Annu. Rev. Biochem. 64*, 897–934.
4. Bachellerie, J. P., Cavaille, J., and Huttenhofer, A. (2002) The expanding snoRNA world. *Biochimie 84*, 775–790.
5. Terns, M. P., and Terns, R. M. (2002) Small nucleolar RNAs: versatile trans-acting molecules of ancient evolutionary origin. *Gene Expression 10*, 17–39.
6. Omer, A. D., Ziesche, S., Decatur, W. A., Fournier, M. J., and Dennis, P. P. (2003) RNA-modifying machines in archaea. *Mol. Microbiol. 48*, 617–629.
7. Meier, T. (2005) The many facets of H/ACA ribonucleoproteins. *Chromosoma 114*, 1–14.
8. Reichow, S. L., Hamma, T., Ferre-D'Amare, A. R., and Varani, G. (2007) The structure and function of small nucleolar ribonucleoproteins. *Nucleic Acids Res. 35*, 1452–1464.
9. Zebarjadian, Y., King, T., Fournier, M. J., Clarke, L., and Carbon, J. (1999) Point mutations in yeast CBF5 can abolish in vivo pseudouridylation of rRNA. *Mol. Cell. Biol. 19*, 7461–7472.
10. Charpentier, B., Muller, S., and Branlant, C. (2005) Reconstitution of archaeal H/ACA small ribonucleoprotein complexes active in pseudouridylation. *Nucleic Acids Res. 33*, 3133–3144.
11. Hamma, T., Reichow, S. L., Varani, G., and Ferre-D'Amare, A. R. (2005) The Cbf5-Nop10 complex is a molecular bracket that organizes box H/ACA RNPs. *Nat. Struct. Mol. Biol. 12*, 1101–1107.
12. Girard, J. P., Lehtonen, H., Caizergues-Ferrer, M., Amalric, F., Tollervey, D., and Lapeyre, B. (1992) GAR1 is an essential small nucleolar RNP protein required for pre-rRNA processing in yeast. *EMBO J. 11*, 673–682.
13. Bousquet-Antonelli, C., Henry, Y. G'Elugne JP., Caizergues-Ferrer, M., and Kiss, T. (1997) A small nucleolar RNP protein is required for pseudouridylation of eukaryotic ribosomal RNAs. *EMBO J. 16* 4770–4776.
14. Lubben, B., Fabrizio, P., Kastner, B., and Luhrmann, R. (1995) Isolation and characterization of the small nucleolar ribonucleoprotein particle snR30 from Saccharomyces cerevisiae. *J. Biol. Chem. 270*, 11549–11554.
15. Lafontaine, D. L., Bousquet-Antonelli, C., Henry, Y., Caizergues-Ferrer, M., and Tollervey, D. (1998) The box H + ACA snoRNAs carry Cbf5p, the putative rRNA pseudouridine synthase. *Genes Dev. 12*, 527–537.
16. Watkins, N. J., Gottschalk, A., Neubauer, G., Kastner, B., Fabrizio, P., Mann, M., and Luhrmann, R. (1998) Cbf5p, a potential pseudouridine synthase, and Nhp2p, a putative RNA-binding protein, are present together with Gar1p in all H BOX/ACA-motif snoRNPs and constitute a common bipartite structure. *RNA 4*, 1549–1568.
17. Henras, A., Henry, Y., Bousquet-Antonelli, C., Noaillac-Depeyre, J., Gelugne, J. P., and Caizergues-Ferrer, M. (1998) Nhp2p and Nop10p are essential for the function of H/ACA snoRNPs. *EMBO J. 17*, 7078–7090.
18. Balakin, A. G., Smith, L., and Fournier, M. J. (1996) The RNA world of the nucleolus: two major families of small RNAs defined by different box elements with related functions. *Cell 86*, 823–834.
19. Ni, J., Tien, A. L., and Fournier, M. J. (1997) Small nucleolar RNAs direct site-specific synthesis of pseudouridine in ribosomal RNA. *Cell 89*, 565–573.
20. Ganot, P., Bortolin, M. L., and Kiss, T. (1997) Site-specific pseudouridine formation in preribosomal RNA is guided by small nucleolar RNAs. *Cell 89*, 799–809.
21. Morrissey, J. P., and Tollervey, D. (1993) Yeast snR30 is a small nucleolar RNA required for 18S rRNA synthesis. *Mol. Cell. Biol. 13*, 2469–2477.
22. Atzorn, V., Fragapane, P., and Kiss, T. (2004) U17/snR30 is a ubiquitous snoRNA with two conserved sequence motifs essential for 18S rRNA production. *Mol. Cell. Biol. 24*, 1769–1778.
23. Mitchell, J. R., Cheng, J., and Collins, K. (1999) A box H/ACA small nucleolar RNA-like domain at the human telomerase RNA 3′ end. *Mol. Cell. Biol. 19*, 567–576.
24. Pogacic, V., Dragon, F., and Filipowicz, W. (2000) Human H/ACA small nucleolar RNPs and telomerase share evolutionarily conserved proteins NHP2 and NOP10. *Mol. Cell. Biol. 20*, 9028–9040.
25. Lukowiak, A. A., Narayanan, A., Li, Z. H., Terns, R. M., and Terns, M. P. (2001) The snoRNA domain of vertebrate telomerase RNA functions to localize the RNA within the nucleus. *RNA 7* 1833–1844.
26. Heiss, N. S., Knight, S. W., Vulliamy, T. J., Klauck, S. M., Wiemann, S., Mason, P. J., Poustka, A., and Dokal, I. (1998) X-linked dyskeratosis congenita is caused by mutations in a highly conserved gene with putative nucleolar functions. *Nat. Genet. 19*, 32–38.
27. Walne, A. J., Vulliamy, T., Marrone, A., Beswick, R., Kirwan, M., Masunari, Y., Al-Qurashi, F. H., Aljurf, M., and Dokal, I. (2007) Genetic heterogeneity in autosomal recessive dyskeratosis congenita with one subtype due to mutations in the telomerase-associated protein NOP10. *Hum. Mol. Genet. 16*, 1619–1629.
28. Vulliamy, T. J., and Dokal, I. (2008) Dyskeratosis congenita: The diverse clinical presentation of mutations in the telomerase complex. *Biochimie 90*, 122–130.
29. Henras, A. K., Capeyrou, R., Henry, Y., and Caizergues-Ferrer, M. (2004) Cbf5p, the putative pseudouridine synthase of H/ACA-type snoRNPs, can form a complex with Gar1p and Nop10p in absence of Nhp2p and box H/ACA snoRNAs. *RNA 10*, 1704–1712.
30. Wang, C., and Meier, U. T. (2004) Architecture and assembly of mammalian H/ACA small nucleolar and telomerase ribonucleoproteins. *EMBO J. 23* 1857–1867.

31. Baker, D. L., Youssef, O. A., Chastkofsky, M. I., Dy, D. A., Terns, R. M., and Terns, M. P. (2005) RNA-guided RNA modification: functional organization of the archaeal H/ACA RNP. *Genes Dev. 19*, 1238–1248.
32. Li, L., and Ye, K. (2006) Crystal structure of an H/ACA box ribonucleoprotein particle. *Nature 443*, 302–307.
33. Sattler, M., Schleucher, J., and Griesinger, C. (1999) Heteronuclear multidimensional NMR experiments for the structure determination of proteins in solution employing pulsed field gradients. *Prog. NMR Spectrosc. 34*, 93–158.
34. Guntert, P. (2004) Automated NMR structure calculation with CYANA. *Methods Mol. Biol. 278*, 353–378.
35. Cornilescu, G., Delaglio, F., and Bax, A. (1999) Protein backbone angle restraints from searching a database for chemical shift and sequence homology. *J. Biomol. NMR 13*, 289–302.
36. Farrow, N. A., Muhandiram, R., Singer, A. U., Pascal, S. M., Kay, C. M., Gish, G., Shoelson, S. E., Pawson, T., Forman-Kay, J. D., and Kay, L. E. (1994) Backbone dynamics of a free and phosphopeptide-complexed Src homology 2 domain studied by 15N NMR relaxation. *Biochemistry 33*, 5984–6003.
37. Mandel, A. M., Akke, M., and Palmer, A. G., 3rd (1995) Backbone dynamics of Escherichia coli ribonuclease HI: correlations with structure and function in an active enzyme. *J. Mol. Biol. 246*, 144–163.
38. Delaglio, F., Grzesiek, S., Vuister, G. W., Zhu, G., Pfeifer, J., and Bax, A. (1995) NMRPipe: a multidimensional spectral processing system based on UNIX pipes. *J. Biomol. NMR 6*, 277–293.
39. Pettersen, E. F., Goddard, T. D., Huang, C. C., Couch, G. S., Greenblatt, D. M., Meng, E. C., and Ferrin, T. E. (2004) UCSF Chimera-a visualization system for exploratory research and analysis. *J. Comput. Chem. 25*, 1605–1612.
40. Koradi, R., Billeter, M., and Wuthrich, K. (1996) MOLMOL: a program for display and analysis of macromolecular structures. *J. Mol. Graphics 14*, 51–55, 29−32.
41. Kabsch, W., and Sander, C. (1983) Dictionary of protein secondary structure: pattern recognition of hydrogen-bonded and geometrical features. *Biopolymers 22*, 2577–2637.
42. Krishnan, V., and Cosman, M. (1998) An empirical relationship between rotational correlation time and solvent accessible surface area. *J. Biomol. NMR 12*, 177–182.
43. Krishna, S. S., Majumdar, I., and Grishin, N. V. (2003) Structural classification of zinc fingers: survey and summary. *Nucleic Acids Res. 31*, 532–550.
44. Manival, X., Charron, C., Fourmann, J. B., Godard, F., Charpentier, B., and Branlant, C. (2006) Crystal structure determination and site-directed mutagenesis of the Pyrococcus abyssi aCBF5-aNOP10 complex reveal crucial roles of the C-terminal domains of both proteins in H/ACA sRNP activity. *Nucleic Acids Res. 34*, 826–839.
45. Ballarino, M., Morlando, M., Pagano, F., Fatica, A., and Bozzoni, I. (2005) The cotranscriptional assembly of snoRNPs controls the biosynthesis of H/ACA snoRNAs in Saccharomyces cerevisiae. *Mol. Cell. Biol. 25*, 5396–5403.
46. Darzacq, X., Kittur, N., Roy, S., Shav-Tal, Y., Singer, R. H., and Meier, U. T. (2006) Stepwise RNP assembly at the site of H/ACA RNA transcription in human cells. *J. Cell Biol. 173*, 207–218.
47. Khanna, M., Wu, H., Johansson, C., Caizergues-Ferrer, M., and Feigon, J. (2006) Structural study of the H/ACA snoRNP components Nop10p and the 3′ hairpin of U65 snoRNA. *RNA 12*, 40–52.
48. Hamma, T., and Ferre-D'Amare, A. R. (2006) Pseudouridine synthases. *Chem. Biol. 13*, 1125–1135.
49. Dragon, F., Pogacic, V., and Filipowicz, W. (2000) In vitro assembly of human H/ACA small nucleolar RNPs reveals unique features of U17 and telomerase RNAs. *Mol. Cell. Biol. 20*, 3037–3048.

BI800418P